THE JOURNAL OF PHYSICAL CHEMISTRY C

Article

pubs.acs.org/JPCC

Hydration of MgO-Based Cement: Water Dynamics by ^{1}H Fast Field-Cycling NMR Relaxometry

Francesca Martini,[†,‡] Silvia Borsacchi,*[,†] Marco Geppi,[†,‡] Claudia Forte,[†] and Lucia Calucci*[,†]

[†]Consiglio Nazionale delle Ricerche – CNR, Istituto di Chimica dei Composti OrganoMetallici, Sede Secondaria di Pisa, via G. Moruzzi 1, 56124 Pisa, Italy

[‡]Dipartimento di Chimica e Chimica Industriale, Università di Pisa, via G. Moruzzi 13, 56124 Pisa, Italy

Supporting Information

ABSTRACT: ^{1}H fast field-cycling (FFC) NMR relaxometry was applied for the first time to monitor the state of water during the hydration reaction of MgO and silica that leads to the formation of magnesium silicate hydrate (M-S-H), the binder phase of innovative cements with promising applications in the containment of radioactive waste. To this aim, water proton longitudinal relaxation rates ($R_1 = 1/T_1$) were measured in the Larmor frequency range between 10 kHz and 30 MHz at different hydration times ranging from 0.5 h to ∼4 months. The obtained R_1 versus frequency (NMRD) curves were analyzed considering fast exchange of water molecules between a hydration layer, where dynamics is affected by interactions with the surface of solids present in the reacting mixture, and a bulk phase. For the hydration layer, water molecules undergoing fast local molecular dynamics on the surface gave a constant contribution to R_1 throughout the investigated frequency range. On the contrary, water molecules undergoing slow dynamics on the surface gave a dispersion of R_1 and their motions were modeled as "reorientations mediated by translational displacements" in the length scale of a particle and of a cluster of particles, where particles are silica nanoparticles and/or M-S-H globules that form during hydration. The model parameters reflected the different typical steps of cement hydration, showing smooth trends in the induction and diffusion steps and sudden changes during the nucleation and growth period in which water is consumed and M-S-H forms.

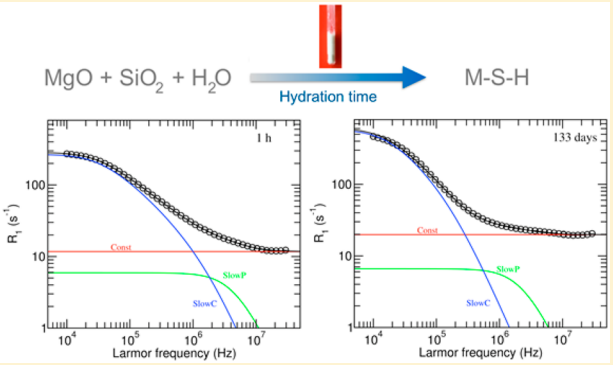

INTRODUCTION

Magnesium silicate hydrate (M-S-H), the phase that forms by the simultaneous hydration of a source of magnesium (typically highly reactive periclase, MgO) and a source of silica (SiO_2), is of interest for several important practical applications.[1−4] In particular, in recent years MgO-based cements have been proposed with the aim of both reducing the environmental footprint associated with the production of traditional Portland cement and developing sustainable fit-for-purpose alternative cements. In fact, the potential use of MgO-based cements in the immobilization of nuclear or metal-containing waste, owing to their lower pH and corrosiveness compared to Portland cement, has been assessed.[5−9] In addition, formation of M-S-H has been found in key environments related to cement applications, such as at the interfacial zone between low-pH Portland-based cements and clays used in multibarrier radioactive waste repositories[10,11] and on the surface of Portland cement pastes and concrete subjected to sulfate attack in the presence of magnesium.[12−15]

The great interest in these applications, and especially in the development of cementitious materials having M-S-H as binder phase, has pushed forward research on the structure of M-S-H. A number of papers on the characterization of M-S-H samples have recently appeared in the literature.[9,16−25] Although there is general agreement in describing M-S-H as a mainly amorphous gel embedding crystalline domains that fail to develop beyond the nanoscale range, several Mg phyllosilicate minerals were proposed to describe the M-S-H structure at the subnanometric scale. In particular, mainly on the basis of ^{29}Si solid state NMR measurements, a mixture of crystalline talc-like and serpentine-like subnanometric domains was found in M-S-H, with one of the two structures prevailing depending on both the Mg/Si ratio and the hydration conditions.[9,16,18−20] The structure of M-S-H at the nanoscale, as resulting from a SAXS study, was described as polydisperse spheres with an average diameter of 3.5 nm and a distribution ranging from 1 to 10 nm arranged into a fractal structure.[17] At the micrometric length scale, SEM images of M-S-H showed an irregular porosity between interconnected and densely packed spherical particles with diameters between 30 and 50 nm.[17,20]

The multiscale structure of the M-S-H gel forms during the hydration process, when MgO and SiO_2 react in the presence of

Received: September 13, 2017
Revised: November 10, 2017
Published: November 10, 2017

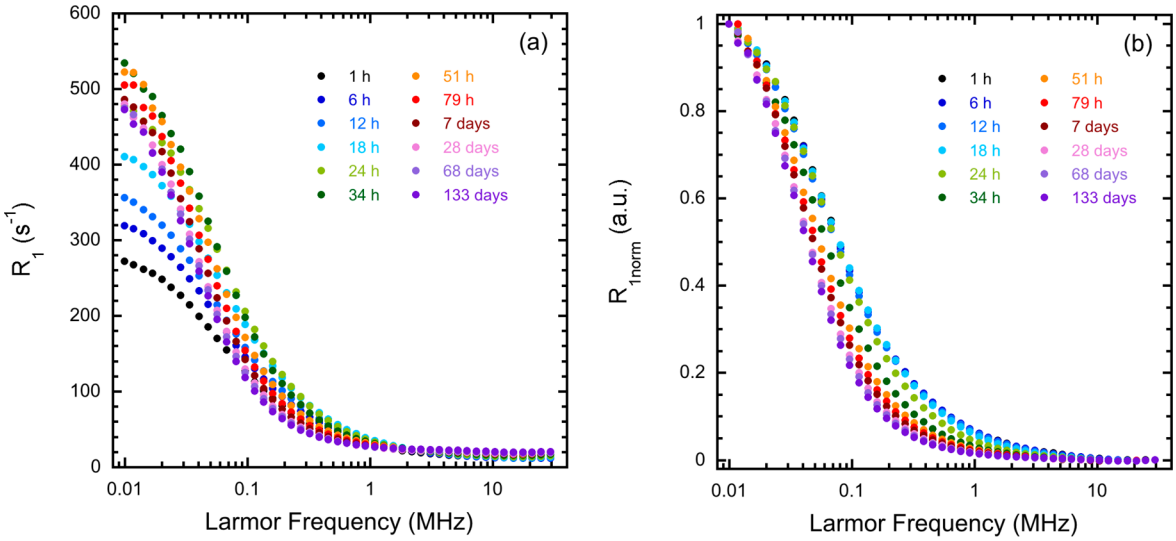

Figure 1. (a) ^{1}H NMRD curves acquired on the $MgO/SiO_2/H_2O$ paste at the indicated hydration times; (b) same curves after normalization according to eq 1.

water, and new solid phases (i.e., M-S-H and, in some cases, $Mg(OH)_2$) precipitate from a supersaturated aqueous solution creating a significant solid−solid bonding interface area in the space that was originally occupied by water. This process gives rise to a porous matrix that evolves in time and causes the paste to set and gain strength. Microstructural properties of the final hardened cement paste, such as porosity, pore size distribution, and specific surface area, have a strong influence on the mechanical properties of cement, as well as on its permeability and durability. Microporous features are in turn strongly related to the state of water in hydrated cement pastes.

Nuclear magnetic resonance (NMR) relaxometry methods, based on the measurement of water proton transverse (T_2) and longitudinal (T_1) relaxation times, offer a variety of opportunities for characterizing water dynamics, and therefore porous microstructure, in cementitious materials through noninvasive approaches that do not require drying nor temperature changes.[26−31] In particular, the dependence of the T_2 values of water protons on the surface-to-volume ratio of pores has been extensively exploited to distinguish and quantify different water populations in the calcium silicate hydrate (C-S-H) gel formed upon hydration of Portland cement.[32−46] Measurement of spin−lattice relaxation rates ($R_1 = 1/T_1$) by means of fast field-cycling (FFC) NMR relaxometry has also been exploited to follow the kinetics of evolution of the specific surface area during the hydration of Portland cement pastes.[26−30,47] In fact, using FFC NMR, R_1 can be measured over a broad range of Larmor frequencies (from 10 kHz to 40 MHz with commercial relaxometers), allowing correlation times for water motions between 1 ns to tens of μs to be probed.[48,49] Besides, length scales explored by this technique range between a few to hundreds of nanometers, largely covering the mesoporous scale.[50] Moreover, the frequency dependence of R_1 in NMR dispersions (NMRD) provides a good test of the theories that relate the measured relaxation rate to the dynamic processes undergone by water molecules in porous matrices and in confined spaces.[27−30,50−59]

In a recent work, ^{1}H T_2 NMR relaxometry was employed for the first time to investigate the hydration process of MgO-based cement.[60] To this aim, T_2 measurements were performed using the Carr−Purcell−Meiboom−Gill (CPMG) pulse sequence[61] at different times, ranging from ∼0.5 h to ∼1 month, during hydration under ambient conditions of a 1:1 molar mixture of highly reactive periclase and fumed silica. The evolution of the distributions of T_2 of water protons, obtained by inversion of the CPMG data with the UPEN algorithm,[62−64] gave information on the kinetics of the hydration reaction, allowing the induction, nucleation and growth, and diffusional steps to be identified, as well as on the formation of the porous structure of the M-S-H phase.

In the present work, ^{1}H FFC NMR relaxometry was applied for the first time to investigate the evolution of water dynamics during the hydration of the same $MgO/SiO_2/H_2O$ paste. To this aim, water proton R_1 was measured as a function of the Larmor frequency in the 0.01−30 MHz range at different hydration times, from 0.5 h to ∼4 months. The resulting NMRD curves were analyzed in terms of models devised for describing the dynamics of fluids embedded in confining systems in order to obtain information on the time evolution of the surface area of the solids during the hydration reaction and of the dynamics of water on the surface.

■ MATERIALS AND METHODS

Sample Preparation. Pastes for ^{1}H FFC NMR measurements were prepared by manually mixing for 10 min highly reactive periclase (MgO >99%, Sigma-Aldrich, reactivity 80 s with the Van der Merwe test,[65] average size 44 μm, BET surface area 121 ± 5 m^2/g) and fumed silica (SiO_2 >99%, Aldrich, average size 5 μm resulting from aggregation/agglomeration of 7 nm primary particles, BET surface area 395 ± 25 m^2/g) in a 1:1 molar ratio and Milli-Q water with a water to solid ratio w/s = 2. Pastes were transferred into NMR tubes immediately after preparation; the tubes were then sealed to avoid water loss and kept at 24 ± 1 °C in a temperature-controlled room. Measurements were performed at different hydration times and the reproducibility of the results was tested by comparing data from two independently prepared samples.

FFC NMR Measurements. ^{1}H and ^{2}H longitudinal relaxation times (T_1) were measured with a Spinmaster FFC-2000 Fast Field-Cycling NMR relaxometer (Stelar srl, Mede, Italy). All measurements were performed at 25 °C and the switching time was 3 ms.

DOI: 10.1021/acs.jpcc.7b09154
J. Phys. Chem. C 2017, 121, 26851−26859

^{1}H T_1 values were measured over the Larmor frequency range 0.01−30 MHz with a 90° pulse duration of 10 μs and a single scan. Measurements were performed using the prepolarized and nonpolarized pulse sequences[48,49] below and above 12 MHz, respectively. The polarizing (B_{pol}) and detection (B_{acq}) fields were 0.70 and 0.50 T, corresponding to ^{1}H Larmor frequencies of 30.0 and 21.5 MHz, respectively. All the ^{1}H magnetization curves versus time, built with at least 16 points, were monoexponential within experimental error; errors on ^{1}H R_1 were less than 2%.

^{2}H T_1 values were measured over the Larmor frequency range 0.013−5.4 MHz with a 90° pulse duration of 22.8 μs and 16 scans. The polarizing (B_{pol}) and detection (B_{acq}) fields were 0.70 and 0.80 T, corresponding to ^{2}H Larmor frequencies of 4.57 and 5.20 MHz, respectively. The ^{2}H magnetization curves vs time, built with 24 points, were monoexponential within experimental error; errors on ^{2}H R_1 were less than 8%.

NMRD curves were analyzed using a least-squares minimization procedure implemented in the Fitteia environment.[66,67]

■ RESULTS AND DISCUSSION

^{1}H FFC NMR experiments were performed on a $MgO/SiO_2/H_2O$ paste at different hydration times in order to measure water proton longitudinal relaxation rates (R_1) as a function of the Larmor frequency in the 0.01−30 MHz range. In all cases only one R_1 value was measured at each frequency; representative NMRD curves are shown in Figure 1a.

At all hydration times, the measured R_1 values were far larger than the relaxation rate of bulk water (∼0.4 s^{-1}), and the NMRD curves showed a quite steep increase of R_1 by decreasing the frequency in the intermediate range around 0.1 MHz, with a plateau at high frequencies (>10 MHz) and a crossover at 20−30 kHz. These trends are characteristic for proton longitudinal relaxation of water confined in diamagnetic porous materials or fine particle agglomerates, that is, confining systems with a large specific surface area presenting a rich variety of shapes.[49−51] However, the NMRD curves showed an evolution during the hydration process. In particular, the R_1 values at the high frequency plateau ranged from ∼12 to ∼21 s^{-1}, slightly decreasing with increasing the hydration time for periods up to ∼8 h, then steeply increasing up to ∼40 h, and increasing with a much lower rate for longer periods. The values of R_1 at frequencies <10 MHz increased with increasing the hydration time up to ∼40 h, and then decreased. The dependence of R_1 on frequency was quite similar for hydration times up to ∼12 h, whereas at longer hydration times changes in the slope of R_1 versus frequency were observed, more marked between 12 h and 2 days. The evolution with hydration time of the frequency dependence of the NMRD curves in the intermediate frequency range is better highlighted after the following normalization procedure is applied to R_1, that is:

$$R_{1\mathrm{norm}}(\omega) = \frac{R_1(\omega) - R_{1\mathrm{plateau}}}{R_{1\mathrm{max}} - R_{1\mathrm{plateau}}} \quad (1)$$

where $R_{1\mathrm{plateau}}$ is the value of R_1 at the high frequency plateau and $R_{1\mathrm{max}}$ is the maximum value of R_1 at low frequency. As reported in Figure 1b for representative hydration times, $R_{1\mathrm{norm}}$ showed superimposable dispersions up to ∼12 h, while at longer hydration times the frequency dependence of the NMRD curves changed, more markedly within few days. This suggests that a dramatic change in the properties of the confining matrix occurs between 12 h and few days.

The evolution of the NMRD curves during the hydration process can be rationalized on the basis of previous results from the free water index (FWI)[24] and ^{1}H T_2[60] measurements. It was found that water is progressively consumed after mixing with MgO and SiO_2, with an acceleration at ∼12 h, when the nucleation and growth period of M-S-H starts, and a deceleration at ∼40 h, when the diffusive period starts. In particular, ∼25% of free water is consumed in the first 40 h, while another ∼8% of water is consumed after 28 days of hydration. Moreover, ^{29}Si solid state NMR, X-ray diffraction, and thermogravimetric data indicated that M-S-H massively forms during the first day of hydration, with consumption of 56% of silica; its content increases by increasing the hydration time at the expense of brucite ($Mg(OH)_2$) and silica, with silica being reduced to about 17% after 7 days and practically absent after 28 days.[20,68]

Quantitative information on water dynamics in the paste during hydration and therefore on the evolution of the M-S-H gel with hydration time was obtained from the analysis of the NMRD curves in terms of models for water proton relaxation in confining systems. In these systems R_1 of water protons is typically expressed considering fast exchange between a hydration layer, where water dynamics is affected by interactions with the surface, and a bulk water phase, these two water phases being associated with spin−lattice relaxation rates $R_{1\mathrm{surf}}$ and $R_{1\mathrm{bulk}}$, respectively.[69] The good overlap of normalized NMRD curves acquired for a paste and a freeze-dried sample (Figure S1), where essentially only the hydration layer contribution remains, indeed showed that the frequency dependence of R_1 is governed by water proton relaxation in the hydration layer, and the measured R_1 results from the weighted average of frequency-dependent $R_{1\mathrm{surf}}$ and frequency-independent $R_{1\mathrm{bulk}}$. While $R_{1\mathrm{bulk}}$ is caused by the modulation of intra- and intermolecular dipolar interactions by fast reorientations and translations, respectively, $R_{1\mathrm{surf}}$ in confining systems is usually dominated by molecular reorientations modulating intramolecular proton dipolar interactions.[49,50] This was here verified by comparing ^{1}H and ^{2}H NMRD curves acquired on samples hydrated with H_2O and D_2O, respectively (Figure 2); the similarity observed between the normalized NMRD curves clearly indicates that relaxation is mainly due to the reorientational modulation of intramolecular interactions, that is the intramolecular dipolar interaction in the case of proton and the quadrupolar interaction in the case of deuterium.

Given the high R_1 values at the high-frequency plateau, much higher than $R_{1\mathrm{bulk}}$, an additional frequency-independent contribution, $R_{1\mathrm{fast}}$, must be considered. It can be hypothesized that $R_{1\mathrm{fast}}$ is the part of $R_{1\mathrm{surf}}$ related to fast local molecular dynamics on the surface. Therefore, R_1 can be written as the sum of three contributions:

$$R_1(\omega) = R_{1\mathrm{bulk}} + R_{1\mathrm{fast}} + R_{1\mathrm{slow}}(\omega) \quad (2)$$

where $R_{1\mathrm{slow}}(\omega)$ is the part of $R_{1\mathrm{surf}}$ that depends on the slow reorientational dynamics of water molecules on the surface giving a dispersion in the investigated frequency range.

For NMR relaxation of water protons in confining systems, mechanisms in which water molecules are adsorbed on and desorbed from the solid surface moving on the surface by translational diffusion and at the same time changing their orientation, have been proposed.[50,51,53,54,56,57] In particular, the "reorientations mediated by translational displacements" model

DOI: 10.1021/acs.jpcc.7b09154
J. Phys. Chem. C 2017, 121, 26851−26859

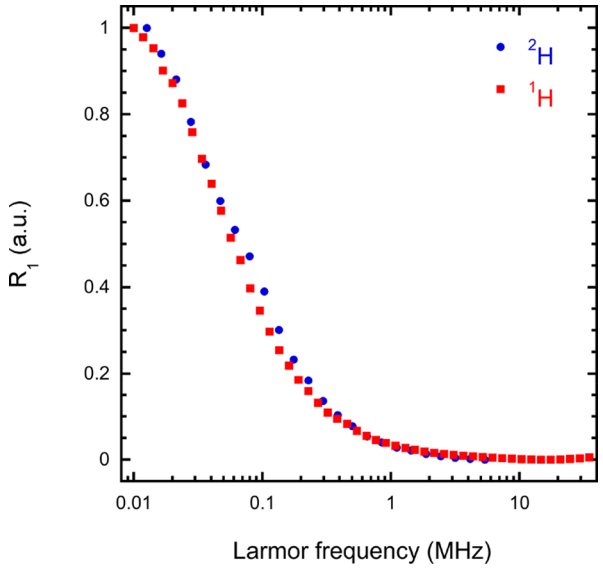

Figure 2. Normalized ^{1}H (red points) and ^{2}H (blue points) NMRD curves acquired on MgO/SiO_2 hydrated for 1 day with H_2O and D_2O, respectively.

(RMTD), in which adsorbate molecules adopt preferential orientations relative to the local surface, has been suggested by Kimmich et al.[50,53,54,56,57] and demonstrated to be valid for several confining systems, such as porous media, particle aggregates, and hydrogels.[54,70−75]

Here, the experimental NMRD curves acquired at different hydration times could be well reproduced considering a constant contribution ($R_{1\mathrm{Const}}$), which includes frequency-independent contributions from bulk water ($R_{1\mathrm{bulk}}$) and water undergoing fast local dynamics ($R_{1\mathrm{fast}}$), and two frequency-dependent contributions arising from slow reorientational motions modeled as RMTD that, following Stapf et al.,[54] can be tentatively ascribed to reorientations in the length scale of a particle ($R_{1\mathrm{slow,P}}(\omega)$) and of a cluster of particles ($R_{1\mathrm{slow,C}}(\omega)$), respectively:

$$R_1(\omega) = R_{1\mathrm{Const}} + R_{1\mathrm{slow,P}}(\omega) + R_{1\mathrm{slow,C}}(\omega) \tag{3}$$

For our system, particles can be tentatively identified with silica nanoparticles but also with M-S-H globules that form during hydration; analogously, clusters of particles can be not only silica nanoparticle aggregates or agglomerates but also densely packed and interconnected globules of M-S-H.

For normal diffusion, the probability density for a water molecule displacement in a given time is expressed by a Gaussian function and can be described in terms of modes with wavenumber k. An exponentially decaying reorientational autocorrelation function for the k mode has an associate characteristic time $\tau_k = (Dk^2)^{-1}$, where D is the translation diffusion coefficient. The spectral density function $J_{k,\mathrm{RMTD}}(\omega)$ for the motion, required to calculate the relaxation rate, is a linear combination of Lorentzian-type contributions of all k modes, weighted by the orientational structure factor $S(k)$, which depends on the surface structure.[49,50,76,77] For small-scale surface structures such as the shape of a single particle, here considered to contribute to $R_{1\mathrm{slow,P}}(\omega)$, the $S(k)$ factor is equal to a Dirac function so that we have a single mode (or a narrow mode distribution) autocorrelation function centered at k_P. The corresponding spectral density can be expressed by a Lorentzian function with correlation time $\tau_{k,\mathrm{P}}$:

$$J_{k,\mathrm{RMTD,P}}(\omega) = \frac{2\tau_{k,\mathrm{P}}}{1 + \omega^2\tau_{k,\mathrm{P}}^2} \tag{4}$$

and[78]

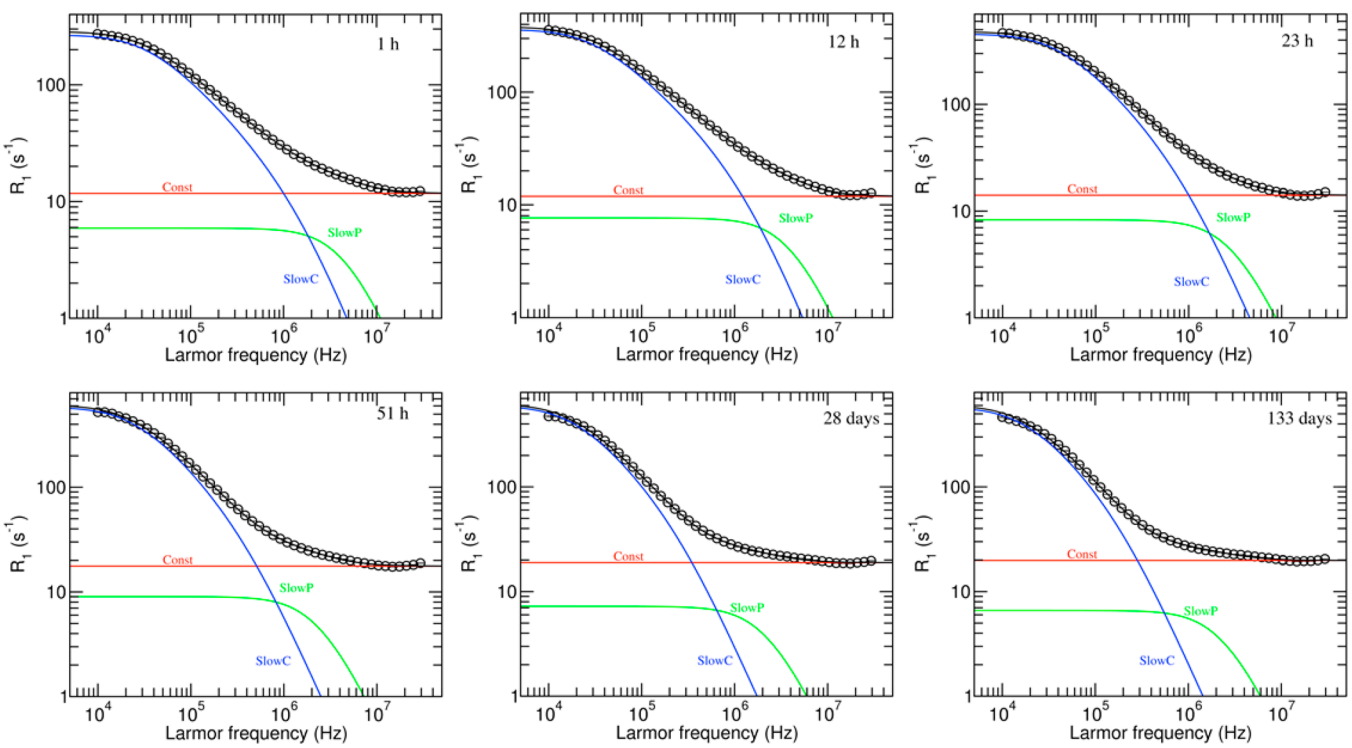

Figure 3. Experimental (circles) and best fit (black lines) ^{1}H NMRD curves obtained for the $MgO/SiO_2/H_2O$ paste at the indicated hydration times. Contributions of $R_{1\mathrm{Const}}$ (red lines), $R_{1\mathrm{slow,P}}$ (green lines), and $R_{1\mathrm{slow,C}}$ (blue lines) to the calculated curves are also shown.

DOI: 10.1021/acs.jpcc.7b09154
J. Phys. Chem. C 2017, 121, 26851−26859

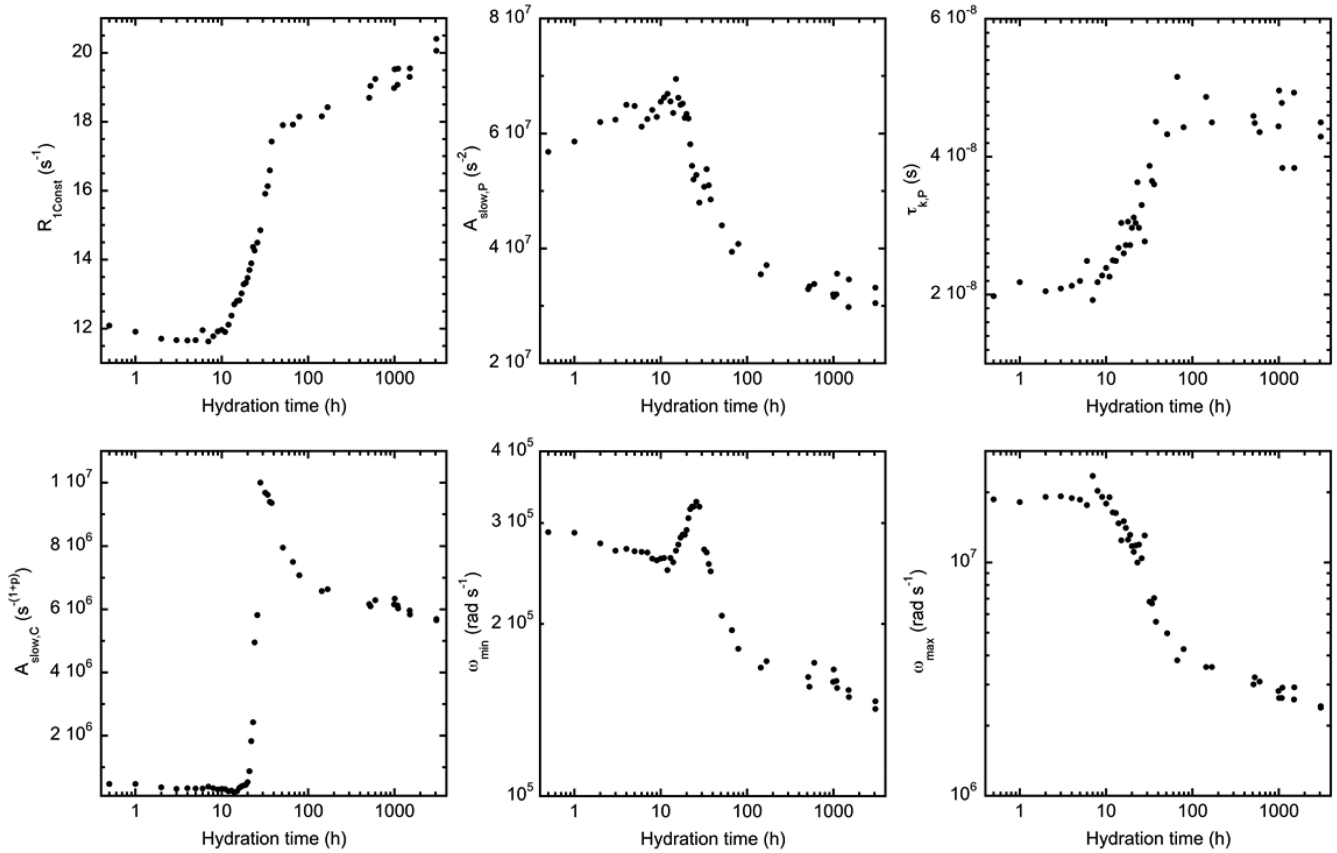

Figure 4. Best fit parameters obtained from the analysis of the experimental ^{1}H NMRD curves acquired on the $MgO/SiO_2/H_2O$ paste at different hydration times.

$$R_{1\mathrm{slow,P}}(\omega) = A_{\mathrm{slow,P}}[J_{k,\mathrm{RMTD,P}}(\omega) + 4J_{k,\mathrm{RMTD,P}}(2\omega)] \quad (5)$$

In the case of particle clusters, the spectral density can be written as

$$J_{k,\mathrm{RMTD,C}}(\omega) = \int_{k_{\min}}^{k_{\max}} S(k)\frac{2\tau_{k,\mathrm{C}}}{1 + \omega^2\tau_{k,\mathrm{C}}^2}\,\mathrm{d}k \quad (6)$$

where $S(k) = ak^{-\chi}$ is the structure factor associated with the microstructural features determined by the network of particles and $k_{\min}$ and $k_{\max}$ are the limit values for the involved modes. Following ref 77, replacing $k\sqrt{D/\omega}$ by z yields

$$J_{k,\mathrm{RMTD,C}}(\omega) = A_{\mathrm{RMTD}}\frac{1}{\omega^p}\int_{z_{\min}}^{z_{\max}} \frac{z^{3-2p}}{1 + z^4}\,\mathrm{d}z \quad (7)$$

with $z_{\min,\max} = (\omega_{\min,\max}/\omega)^{1/2}$, $\omega_{\min,\max} = 1/\tau_{k_{\max,\min,\mathrm{C}}} = Dk^2{}_{\min,\max}$, and $p = (1 + \chi)/2$, and[78]

$$R_{1\mathrm{slow,C}}(\omega) = A_{\mathrm{slow,C}}[J_{k,\mathrm{RMTD,C}}(\omega) + 4J_{k,\mathrm{RMTD,C}}(2\omega)] \quad (8)$$

It must be noted that the dispersion contribution follows the power law $R_{1\mathrm{slow,C}} \propto \omega^{-(1+\chi)/2}$. $A_{\mathrm{slow,P}}$ and $A_{\mathrm{slow,C}}$ in eqs 5 and 8 are factors depending on the residual dipole−dipole proton interactions and on the fractional water populations associated with the two slow relaxation mechanisms.

Experimental NMRD curves could be well reproduced taking into account the different contributions to proton relaxation (eq 3) and expressing the relaxation rates $R_{1\mathrm{slow,P}}(\omega)$ and $R_{1\mathrm{slow,C}}(\omega)$ as in eqs 5 and 8, respectively; examples of calculated curves are shown in Figure 3. Seven parameters (i.e., $R_{1\mathrm{Const}}$, $A_{\mathrm{slow,P}}$, $\tau_{k,\mathrm{P}}$, p, $A_{\mathrm{slow,C}}$, $\omega_{\min}$, and $\omega_{\max}$) were determined by fitting the NMRD curves with the model at each hydration time; best fitting values of $R_{1\mathrm{Const}}$, $A_{\mathrm{slow,P}}$, $\tau_{k,\mathrm{P}}$, $A_{\mathrm{slow,C}}$, $\omega_{\min}$, and $\omega_{\max}$ are reported in Figure 4.

In the interpretation of the data, it must be borne in mind that the system investigated is undergoing chemical and structural changes upon hydration. In fact, at the beginning of the hydration process, MgO dissolves in water giving Mg^{2+} and OH^- ions. When a saturation concentration is reached, brucite precipitates, and a moderately basic pH is established ($pK_a \cong 10.5$) that favors hydration of silica with formation of silicate anions. Then, Mg^{2+} and silicate ions react to form M-S-H. The trend of $R_{1\mathrm{Const}}$ as a function of time shows a slight decrease for times up to 8 h, a steep increase between 10 and 40 h, and a more gradual increase afterward. This trend can be related to the consumption of water, mainly bulk water, and the formation of the M-S-H phase during the different stages of the hydration process. However, it could also be due to a slowing down of water motions with the formation of the new phase, although these motions remain fast with respect to the investigated frequency range. $A_{\mathrm{slow,P}}$ slightly increases for hydration times up to 12 h, then decreases rapidly between 12 and 50 h and more smoothly at longer times; this behavior can be accounted for with a reduction of water molecules interacting with the surface over a single particle length scale, thus indicating the formation of a more extended structure in which water is embedded. Correspondingly, the factor $A_{\mathrm{slow,C}}$ remains practically constant up to 20 h, rapidly increases between 20 and 30 h, and decreases for longer hydration periods. This trend can be associated not only with an increase

DOI: 10.1021/acs.jpcc.7b09154
J. Phys. Chem. C 2017, 121, 26851−26859

of the water fraction interacting with the surface of the particle clusters, and in particular of the spherical particle agglomerates characteristic of the M-S-H phase, but also with the change of the power law dependence of $R_{1slow,C}$ on frequency. In fact, the exponent p is equal to 0.76 ± 0.05 for hydration times up to 20 h, rapidly increases up to 1 between 20 and 30 h, remaining constant until the longest hydration time monitored. Considering the relationship between χ and the fractal dimensionality of clusters, $\chi = 3 - D_f$, reported by Zavada et al.,[57] the variation of p can be associated with a change of the fractal dimensionality from 2.48 to 2 on passing from the reactants to M-S-H, suggesting a smoothing of the surface. The trend of $\tau_{k,P}$ with hydration time indicates a sudden increase of the correlation time for the associated water reorientations on the surface when M-S-H forms. Both ω_{min} and ω_{max} values show a general decreasing trend with hydration time, which becomes more rapid between 20 and 60 h. The maximum correlation time $\tau_{k_{max},C}$ represents the residence time of the water molecules on the solid surface, after which a water molecule completely loses contact with the surface and diffuses in the bulk. The minimum correlation time $\tau_{k_{min},C}$ represents the residence time of a water molecule on a surface site during its stay on the surface. Values of $\tau_{k_{max},C}$ and $\tau_{k_{min},C}$ were found ∼3 and ∼0.05 μs, respectively, at early hydration times, while they were ∼7 and ∼0.4 μs at the latest ones. These values indicate that both the residence time of water on the surface and the time between water molecule jumps between surface sites are longer for M-S-H than for silica nanoparticles.

An estimate of the length scale associated with the reorientational processes discussed above can be obtained under certain assumptions. Considering the Einstein−Smoluchowski relation for a two-dimensional movement with a diffusion coefficient D, $\langle r^2 \rangle = 4D\tau$, we can associate mean water displacements to correlation times. In particular, assuming $D = 2.3\times10^{-9}$ m^2/s, equal to the translational diffusion coefficient of water at 25 °C,[79] values of the mean water displacement associated with $\tau_{k,P}$ ranging from ∼14 to ∼21 nm on going from the reactants to the M-S-H phase at the end of the hydration period were estimated. An increase of the mean water displacement during the hydration process was also found for reorientations on clusters. In particular, displacements associated with $\tau_{k_{min},C}$ were ∼22 nm at the beginning of hydration and ∼60 nm at the end, while those associated with $\tau_{k_{max},C}$ were ∼180 nm and ∼250 nm at early and latest hydration times, respectively.

The "molecular intermittent dynamics" model, in which the trajectory of fluid molecules near the interface is described as an alternate succession of adsorption steps and random walks in the bulk until definitive loss by adsorption or final escaping at the interface, as presented by Levitz et al.[51] and successfully applied to investigate water dynamics in different confining systems,[51,80−85] could also satisfactorily reproduce the low and intermediate frequency range of our experimental NMRD curves. However, it failed in reproducing the curves leveling off at low frequencies, as also observed by other authors.[76,81,82]

CONCLUSIONS

FFC NMR revealed to be a valuable technique for giving detailed information on the dynamics of water during the hydration process of a $MgO/SiO_2/H_2O$ paste of great interest for the development of MgO-based cements, as well as of refractory MgO-based materials, catalysts, and adsorbents. The interaction of water with the surface of fumed silica nanoparticles, at the beginning of the hydration process, and with a complex and time evolving mixture constituted by unreacted silica, brucite, and M-S-H gel as the hydration process proceeds, could be monitored following the evolution of the NMRD curves, which are dominated by water molecule reorientations on the solid surfaces. Parameters characterizing the surface/water interactions could be determined by fitting the curves to a model including contributions from water molecules undergoing fast motions and water molecules reorienting while diffusing on the surface of the solid matrix (RMTD model). The results point to a progressive consumption of water during the hydration and an increase of the water fraction interacting with the solid surface, and therefore of the surface to volume ratio in the paste on passing from reactants to M-S-H. Moreover, longer correlation times and therefore longer mean displacements were found for water molecules on the surface of M-S-H with respect to silica. Our findings give a significant contribution to the present knowledge of a complex material, such as M-S-H, and can be of aid in understanding the relationship between microscopic and macroscopic properties.

ASSOCIATED CONTENT

Supporting Information

The Supporting Information is available free of charge on the ACS Publications website at DOI: 10.1021/acs.jpcc.7b09154.

^{1}H NMRD of a freeze-dried $MgO/SiO_2/H_2O$ paste after 28 days of hydration (PDF)

AUTHOR INFORMATION

Corresponding Authors

*Phone: +39-0503153052. E-mail: silvia.borsacchi@pi.iccom.cnr.it.

*Phone: +39-0503152517. E-mail: lucia.calucci@pi.iccom.cnr.it.

ORCID

Claudia Forte: 0000-0003-0405-2038

Lucia Calucci: 0000-0002-3080-8807

Notes

The authors declare no competing financial interest.

ACKNOWLEDGMENTS

This work was performed with the financial support of Ministero dell'Istruzione, Università e Ricerca scientifica (MIUR), FIR2013 Project RBFR132WSM. Francesca Ridi and Monica Tonelli (Università di Firenze) are kindly acknowledged for helpful discussions.

ABBREVIATIONS

FFC, Fast Field-Cycling; M-S-H, Magnesium Silicate Hydrate; NMRD, Nuclear Magnetic Relaxation Dispersion; RMTD, Reorientations Mediated by Translational Displacements

REFERENCES

(1) Walling, S. A.; Provis, J. L. Magnesia-Based Cements: A Journey of 150 Years, and Cements for the Future? *Chem. Rev.* **2016**, *116*, 4170−4204.

(2) Szczerba, J.; Prorok, R.; Śnieżek, E.; Madej, D.; Maślona, K. Influence of Time and Temperature on Ageing and Phases Synthesis in the $MgO-SiO_2-H_2O$ System. *Thermochim. Acta* **2013**, *567*, 57−64.

DOI: 10.1021/acs.jpcc.7b09154
J. Phys. Chem. C 2017, 121, 26851−26859

(3) Huang, R.; Wu, M.; Zhang, T.; Li, D.; Tang, P.; Feng, Y. Template-free Synthesis of Large-Pore-Size Porous Magnesium Silicate Hierarchical Nanostructures for High-Efficiency Removal of Heavy Metal Ions. *ACS Sustainable Chem. Eng.* **2017**, *5*, 2774−2780.
(4) Chung, S.-H.; Angelici, C.; Hinterding, S. O. M.; Weingarth, M.; Baldus, M.; Houben, K.; Weckhuysen, B. M.; Bruijnincx, P. C. A. Role of Magnesium Silicates in Wet-Kneaded Silica-Magnesia Catalysts for the Lebedev Ethanol-to-Butadiene Process. *ACS Catal.* **2016**, *6*, 4034−4045.
(5) Zhang, T.; Cheeseman, C. R.; Vandeperre, L. J. Development of Low pH Cement Systems Forming Magnesium Silicate Hydrate (M-S-H). *Cem. Concr. Res.* **2011**, *41*, 439−442.
(6) Zhang, T.; Vandeperre, L. J.; Cheeseman, C. Bottom-up Design of a Cement for Nuclear Waste Encapsulation. In *Ceramic Materials for Energy Applications*; John Wiley & Sons, Inc.: New York, 2011; pp 41−49.
(7) Zhang, T.; Cheeseman, C.; Vandeperre, L. J. Characterisation of Corrosion of Nuclear Metal Wastes Encapsulated in Magnesium Silicate Hydrate (MSH) Cement. In *Ceramic Materials for Energy Applications II*; John Wiley & Sons, Inc.: New York, 2012; pp 159−167.
(8) Zhang, T.; Vandeperre, L. J.; Cheeseman, C. R. Magnesium-Silicate-Hydrate Cements for Encapsulating Problematic Aluminium Containing Wastes. *J. Sustainable Cem.-Based Mater.* **2012**, *1*, 34−45.
(9) Walling, S. A.; Kinoshita, H.; Bernal, S. A.; Collier, N. C.; Provis, J. L. Structure and Properties of Binder Gels Formed in the System $Mg(OH)_2$-SiO_2-H_2O for Immobilisation of Magnox Sludge. *Dalton Trans.* **2015**, *44*, 8126−8137.
(10) Dauzeres, A.; Achiedo, G.; Nied, D.; Bernard, E.; Alahrache, S.; Lothenbach, B. Magnesium Perturbation in Low-pH Concretes Placed in Clay Environment-Solid Characterizations and Modeling. *Cem. Concr. Res.* **2016**, *79*, 137−150.
(11) Jenni, A.; Madër, U.; Lerouge, C.; Gaboreau, S.; Schwyn, B. In Situ Interaction Between Different Concretes and Opalinus Clay. *Phys. Chem. Earth* **2014**, *70−71*, 71−83.
(12) Bonen, D.; Cohen, M. D. Magnesium Sulfate Attack on Portland Cement Paste-I. Microstructural Analysis. *Cem. Concr. Res.* **1992**, *22*, 169−180.
(13) Bonen, D.; Cohen, M. D. Magnesium Sulfate Attack on Portland Cement Paste-II. Chemical and Mineralogical Analyses. *Cem. Concr. Res.* **1992**, *22*, 707−718.
(14) Bonen, D. Composition and Appearance of Magnesium Silicate Hydrate and its Relation to Deterioration of Cement-Based Materials. *J. Am. Ceram. Soc.* **1992**, *75*, 2904−2906.
(15) Gollop, R.; Taylor, H. Microstructural and Microanalytical Studies of Sulfate Attack. IV Reactions of a Slag Cement Paste with Sodium and Magnesium Sulfate Solutions. *Cem. Concr. Res.* **1996**, *26*, 1013−1028.
(16) Brew, D. R. M.; Glasser, F. P. Synthesis and Characterisation of Magnesium Silicate Hydrate Gels. *Cem. Concr. Res.* **2005**, *35*, 85−98.
(17) Chiang, W.-S.; Ferraro, G.; Fratini, E.; Ridi, F.; Yeh, Y.-Q.; Jeng, U.-S.; Chen, S.-H.; Baglioni, P. Multiscale Structure of Calcium- and Magnesium-Silicate-Hydrate Gels. *J. Mater. Chem. A* **2014**, *2*, 12991−12998.
(18) Roosz, C.; Grangeon, S.; Blanc, P.; Montouillout, V.; Lothenbach, B.; Henocq, P.; Giffaut, E.; Vieillard, P.; Gaboreau, S. Crystal Structure of Magnesium Silicate Hydrates (M-S-H): The Relation with 2:1 Mg−Si Phyllosilicates. *Cem. Concr. Res.* **2015**, *73*, 228−237.
(19) Lothenbach, B.; Nied, D.; L'Hôpital, E.; Achiedo, G.; Dauzères, A. Magnesium and Calcium Silicate Hydrates. *Cem. Concr. Res.* **2015**, *77*, 60−68.
(20) Tonelli, M.; Martini, F.; Calucci, L.; Fratini, E.; Geppi, M.; Ridi, F.; Borsacchi, S.; Baglioni, P. Structural Characterization of Magnesium Silicate Hydrate: Towards the Design of Eco-Sustainable Cements. *Dalton Trans.* **2016**, *45*, 3294−3304.
(21) Le, P.; Fratini, E.; Ito, K.; Wang, Z.; Mamontov, E.; Baglioni, P.; Chen, S.-H. Dynamical Behaviors of Structural, Constrained and Free Water in Calcium- and Magnesium-Silicate-Hydrate Gels. *J. Colloid Interface Sci.* **2016**, *469*, 157−163.
(22) Chen, J.; Li, T.; Li, X.; Chou, K.-C.; Hou, X. Some New Perspective on the Reaction Mechanism of MgO-SiO_2-H_2O System. *Int. J. Appl. Ceram. Technol.* **2016**, *13*, 1164−1172.
(23) Tran, H. M.; Scott, A. Strength and Workability of Magnesium Silicate Hydrate Binder Systems. *Constr. Build. Mater.* **2017**, *131*, 526−535.
(24) Tonelli, M.; Martini, F.; Calucci, L.; Geppi, M.; Borsacchi, S.; Ridi, F. Traditional Portland Cement and MgO-based Cement: a Promising Combination? *Phys. Chem. Earth.* **2017**, *99*, 158−167.
(25) Bernard, E.; Lothenbach, B.; Rentsch, D.; Pochard, I.; Dauzères, A. Formation of Magnesium Silicate Hydrates (M-S-H). *Phys. Chem. Earth.* **2017**, *99*, 142−157.
(26) Barberon, F.; Korb, J.-P.; Petit, D.; Morin, V.; Bermejo, E. Probing the Surface Area of a Cement-Based Material by Nuclear Magnetic Relaxation Dispersion. *Phys. Rev. Lett.* **2003**, *90*, 116103.
(27) Plassais, A.; Pomiès, M.-P.; Lequeux, N.; Korb, J.-P.; Petit, D.; Barberon, F.; Bresson, B. Microstructure Evolution of Hydrated Cement Pastes. *Phys. Rev. E* **2005**, *72*, 041401.
(28) Korb, J.-P. NMR and Nuclear Spin Relaxation of Cement and Concrete Materials. *Curr. Opin. Colloid Interface Sci.* **2009**, *14*, 192−202.
(29) Korb, J.-P. Nuclear Magnetic Relaxation of Liquids in Porous Media. *New J. Phys.* **2011**, *13*, 035016.
(30) Valori, A.; McDonald, P. J.; Scrivener, K. L. The Morphology of C-S-H: Lessons from ^{1}H Nuclear Magnetic Resonance Relaxometry. *Cem. Concr. Res.* **2013**, *49*, 65−81.
(31) Bortolotti, V.; Brizi, L.; Brown, R. J. S.; Fantazzini, P.; Mariani, M. Nano and Sub-nano Multiscale Porosity Formation and Other Features Revealed by ^{1}H NMR Relaxometry During Cement Hydration. *Langmuir* **2014**, *30*, 10871−10877.
(32) McDonald, P. J.; Rodin, V.; Valori, A. Characterization of Intra- and Inter-C-S-H Gel Pore Water in White Cement Based on an Analysis of NMR Signal Amplitudes as a Function of Water Content. *Cem. Concr. Res.* **2010**, *40*, 1656−1663.
(33) Muller, A. C. A.; Scrivener, K. L.; Gajewicz, A. M.; McDonald, P. J. Use of Bench-top NMR to Measure the Density, Composition and Desorption Isotherm of C-S-H in Cement Paste. *Microporous Mesoporous Mater.* **2013**, *178*, 99−103.
(34) Pop, A.; Badea, C.; Ardelean, I. The Effects of Different Superplasticizers and Water-to-Cement Ratios on the Hydration of Gray Cement using T_2-NMR. *Appl. Magn. Reson.* **2013**, *44*, 1223−1234.
(35) Bligh, M. W.; d'Eurydice, M. N.; Lloyd, R. R.; Arns, C. H.; Waite, T. D. Investigation of Early Hydration Dynamics and Microstructural Development of Ordinary Portland Cement Using ^{1}H NMR Relaxometry and Isothermal Calorimetry. *Cem. Concr. Res.* **2016**, *83*, 131−139.
(36) Halperin, W. P.; Jehng, J.-Y.; Song, Y.-Q. Application of Spin-Spin Relaxation to Measurement of Surface Area and Pore Size Distributions in a Hydrating Cement Paste. *Magn. Reson. Imaging* **1994**, *12*, 169−173.
(37) Gombia, M.; Bortolotti, V.; De Carlo, B.; Mongiorgi, R.; Zanna, S.; Fantazzini, P. Nanopore Structure Buildup during Endodontic Cement Hydration Studied by Time-Domain Nuclear Magnetic Resonance of Lower and Higher Mobility ^{1}H. *J. Phys. Chem. B* **2010**, *114*, 1767−1774.
(38) Muller, A. C. A.; Scrivener, K. L.; Gajewicz, A. M.; McDonald, P. J. Densification of C-S-H Measured by ^{1}H NMR Relaxometry. *J. Phys. Chem. C* **2013**, *117*, 403−412.
(39) Greener, J.; Peemoeller, H.; Choi, C.; Holly, R.; Reardon, E. J.; Hansson, C. M.; Pintar, M. M. Monitoring of Hydration of White Cement Paste with Proton NMR Spin-Spin Relaxation. *J. Am. Ceram. Soc.* **2000**, *83*, 623−627.
(40) Bortolotti, V.; Brown, R. J. S.; Fantazzini, P.; Mariani, M. Evolution of a Short-T2 Liquid-Like ^{1}H Signal during the Hydration of White Portland Cement. *Microporous Mesoporous Mater.* **2013**, *178*, 108−112.

DOI: 10.1021/acs.jpcc.7b09154
J. Phys. Chem. C 2017, 121, 26851−26859

(41) Díaz-Díaz, F.; de J. Cano-Barrita, P. F.; Balcom, B. J.; Solís-Nájera, S. E.; Rodríguez, A. O. Embedded NMR Sensor to Monitor Compressive Strength Development and Pore Size Distribution in Hydrating Concrete. *Sensors* **2013**, *13*, 15985−15999.
(42) Pop, A.; Ardelean, I. Monitoring the Size Evolution of Capillary Pores in Cement Paste During the Early Hydration via Diffusion in Internal Gradients. *Cem. Concr. Res.* **2015**, *77*, 76−81.
(43) Stepišnik, J.; Ardelean, I. Usage of Internal Magnetic Fields to Study the Early Hydration Process of Cement Paste by MGSE Method. *J. Magn. Reson.* **2016**, *272*, 100−107.
(44) Bede, A.; Scurtu, A.; Ardelean, I. NMR Relaxation of Molecules Confined Inside the Cement Paste Pores Under Partially Saturated Conditions. *Cem. Concr. Res.* **2016**, *89*, 56−62.
(45) Muller, A. C. A.; Scrivener, K. L.; Skibsted, J.; Gajewicz, A. M.; McDonald, P. J. Influence of Silica Fume on the Microstructure of Cement Pastes: New Insights from ^{1}H NMR Relaxometry. *Cem. Concr. Res.* **2015**, *74*, 116−125.
(46) Gajewicz, A. M.; Gartner, E.; Kang, K.; McDonald, P. J.; Yermakou, V. A ^{1}H NMR Relaxometry Investigation of Gel-Pore Drying Shrinkage in Cement Pastes. *Cem. Concr. Res.* **2016**, *86*, 12−19.
(47) Badea, C.; Pop, A.; Mattea, C.; Stapf, S.; Ardelean, I. The Effect of Curing Temperature on Early Hydration of Gray Cement Via Fast Field Cycling-NMR. *Appl. Magn. Reson.* **2014**, *45*, 1299−1309.
(48) Anoardo, E.; Galli, G.; Ferrante, G. Fast-Field-Cycling NMR: Applications and Instrumentation. *Appl. Magn. Reson.* **2001**, *20*, 365−404.
(49) Kimmich, R.; Anoardo, E. Field-Cycling NMR Relaxometry. *Prog. Nucl. Magn. Reson. Spectrosc.* **2004**, *44*, 257−320.
(50) Kimmich, R. Strange Kinetics, Porous Media, and NMR. *Chem. Phys.* **2002**, *284*, 253−285.
(51) Levitz, P. Random Flights in Confining Interfacial Systems. *J. Phys.: Condens. Matter* **2005**, *17*, S4059−S4074.
(52) Levitz, P.; Bonnaud, P. A.; Cazade, P.-A.; Pellenq, R. J.-M.; Coasne, B. Molecular Intermittent Dynamics of Interfacial Water: Probing Adsorption and Bulk Confinement. *Soft Matter* **2013**, *9*, 8654−8663.
(53) Kimmich, R.; Weber, H. W. NMR Relaxation and the Orientational Structure Factor. *Phys. Rev. B: Condens. Matter Mater. Phys.* **1993**, *47*, 11788−11794.
(54) Stapf, S.; Kimmich, R.; Niess, J. Microstructure of Porous Media and Field-Cycling Nuclear Magnetic Relaxation Spectroscopy. *J. Appl. Phys.* **1994**, *75*, 529−537.
(55) Stapf, S.; Kimmich, R.; Seitter, R.-O. Proton and Deuteron Field-Cycling NMR Relaxometry of Liquids in Porous Glasses: Evidence for Lévy-Walk Statistics. *Phys. Rev. Lett.* **1995**, *75*, 2855−2858.
(56) Zavada, T.; Kimmich, R. The Anomalous Adsorbate Dynamics at Surfaces in Porous Media Studied by Nuclear Magnetic Resonance Methods. The Orientational Structure Factor and Lévy Walks. *J. Chem. Phys.* **1998**, *109*, 6929−6939.
(57) Zavada, T.; Kimmich, R. Surface Fractals Probed by Adsorbate Spin-Lattice Relaxation Dispersion. *Phys. Rev. E: Stat. Phys., Plasmas, Fluids, Relat. Interdiscip. Top.* **1999**, *59*, 5848−5854.
(58) Faux, D. A.; McDonald, P. J.; Howlett, N. C. Nuclear-Magnetic-Resonance Relaxation Due to the Translational Diffusion of Fluid Confined to Quasi-Two-Dimensional Pores. *Phys. Rev. E: Stat. Phys., Plasmas, Fluids, Relat. Interdiscip. Top.* **2017**, *95*, 033116.
(59) Faux, D. A.; McDonald, P. J. Explicit Calculation of Nuclear-Magnetic-Resonance Relaxation Rates in Small Pores to Elucidate Molecular-Scale Fluid Dynamics. *Phys. Rev. E: Stat. Phys., Plasmas, Fluids, Relat. Interdiscip. Top.* **2017**, *95*, 033117.
(60) Martini, F.; Borsacchi, S.; Geppi, M.; Tonelli, M.; Ridi, F.; Calucci, L. Monitoring the Hydration of MgO-Based Cement and Its Mixtures with Portland Cement by ^{1}H NMR Relaxometry. *Microporous Mesoporous Mater.* **2017**, DOI: 10.1016/j.micromeso.2017.05.031.
(61) Meiboom, S.; Gill, D. Modified Spin-Echo Method for Measuring Nuclear Relaxation Times. *Rev. Sci. Instrum.* **1958**, *29*, 688−691.
(62) Borgia, G. C.; Brown, R. J. S.; Fantazzini, P. Uniform-Penalty Inversion of Multiexponential Decay Data. *J. Magn. Reson.* **1998**, *132*, 65−77.
(63) Borgia, G. C.; Brown, R. J. S.; Fantazzini, P. Uniform-Penalty Inversion of Multiexponential Decay Data: II. Data Spacing, T2 Data, Systematic Data Errors, and Diagnostics. *J. Magn. Reson.* **2000**, *147*, 273−285.
(64) Borgia, G. C.; Brown, R. J. S.; Fantazzini, P. Examples of Marginal Resolution of NMR Relaxation Peaks Using UPEN and Diagnostics. *Magn. Reson. Imaging* **2001**, *19*, 473−475.
(65) Van der Merwe, E. M.; Strydom, C.; Botha, A. Hydration of Medium Reactive Industrial Magnesium Oxide with Magnesium Acetate. *J. Therm. Anal. Calorim.* **2004**, *77*, 49−56.
(66) Sebastião, P. J. Fitteia. Fitting Environment Interfaces for All. http://fitteia.org (accessed on September 10, 2017).
(67) Sebastião, P. J. The Art of Model Fitting to Experimental Results. *Eur. J. Phys.* **2014**, *35*, 015017.
(68) Martini, F.; Tonelli, M.; Geppi, M.; Ridi, F.; Borsacchi, S.; Calucci, L. Hydration of MgO/SiO_2 and Portland Cement Mixtures: a Structural Investigation of the Hydrated Phases by Means of X-Ray Diffraction and Solid State NMR Spectroscopy. *Cem. Concr. Res.* **2017**, *102*, 60−67.
(69) Brownstein, K. R.; Tarr, C. E. Importance of Classical Diffusion in NMR Studies of Water in Biological Cells. *Phys. Rev. A: At., Mol., Opt. Phys.* **1979**, *19*, 2446−2453.
(70) Stapf, S.; Kimmich, R.; Seitter, R.-O.; Maklakov, A. I.; Skirda, V. D. Proton and Deuteron Field-Cycling NMR Relaxometry of Liquids Confined in Porous Glasses. *Colloids Surf., A* **1996**, *115*, 107−114.
(71) Zavada, T.; Kimmich, R.; Stapf, S. NMR Experiments on Molecular Dynamics in Nanoporous Media: Evidence for Lévy Walk Statistics. *MRS Online Proc. Libr.* **1996**, *464*, 313−324.
(72) Zavada, T.; Kimmich, R.; Grandjean, J.; Kobelkov, A. Field-Cycling NMR Relaxometry of Water in Synthetic Saponites: Lévy Walks on Finite Planar Surfaces. *J. Chem. Phys.* **1999**, *110*, 6977−6981.
(73) Carvalho, A.; Sebastião, P. J.; Fonseca, I.; Matos, J.; Gonçalves, M. C. Silica and Silica Organically Modified Nanoparticles: Water Dynamics in Complex Systems. *Microporous Mesoporous Mater.* **2015**, *217*, 102−108.
(74) Silletta, E. V.; Velasco, M. I.; Gomez, C. G.; Strumia, M. C.; Stapf, S.; Mattea, C.; Monti, G. A.; Acosta, R. H. Enhanced Surface Interaction of Water Confined in Hierarchical Porous Polymers Induced by Hydrogen Bonding. *Langmuir* **2016**, *32*, 7427−7434.
(75) Tritt-Goc, J.; Rachocki, A.; Bielejewski, M. The Solvent Dynamics at Pore Surfaces in Molecular Gels Studied by Field-Cycling Magnetic Resonance Relaxometry. *Soft Matter* **2014**, *10*, 7810−7818.
(76) Sebastião, P. J.; Sousa, D.; Ribeiro, A. C.; Vilfan, M.; Lahajnar, G.; Seliger, J.; Žumer, S. Field-Cycling NMR Relaxometry of a Liquid Crystal above T_{NI} in Mesoscopic Confinement. *Phys. Rev. E* **2005**, *72*, 061702.
(77) Vilfan, M.; Apih, T.; Sebastião, P. J.; Lahajnar, G.; Žumer, S. Liquid Crystal 8CB in Random Porous Glasses: NMR Relaxometry Study of Molecular Diffusion and Director Fluctuations. *Phys. Rev. E* **2007**, *76*, 051708.
(78) Bloembergen, N.; Purcell, E. M.; Pound, R. V. Relaxation Effects in Nuclear Magnetic Absorption. *Phys. Rev.* **1948**, *73*, 679−712.
(79) Holz, M.; Heil, S. R.; Sacco, A. Temperature-Dependent Self-Diffusion Coefficients of Water and Six Selected Molecular Liquids for Calibration in Accurate ^{1}H NMR PFG Measurements. *Phys. Chem. Chem. Phys.* **2000**, *2*, 4740−4742.
(80) Levitz, P. E.; Korb, J.-P. Probing Glass Transition of Clay Colloids by NMR Relaxometry: Interplay between Fluid Brownian Dynamics and Particle Jamming. *Europhys. Lett.* **2005**, *70*, 684−689.
(81) Korb, J.-P.; Levitz, P. Direct Probing of the Wettability of Plaster Phases at the Nanoscale by Proton Field Cycling Relaxometry. In *Magnetic Resonance in Porous Media: Proceedings of the 9th International Bologna Conference on Magnetic Resonance in Porous Media (MRPM9), including 8th Colloquium on Mobile Magnetic Resonance (CMMR8)*;

DOI: 10.1021/acs.jpcc.7b09154
J. Phys. Chem. C 2017, 121, 26851−26859

Hurlimann, M. D., Song, Y. D., Fantazzini, P., Bortolotti, V., Eds.; AIP Conference Proceedings, 2008; Vol. *1081*, pp 55−58.
(82) Levitz, P.; Zinsmeister, M.; Davidson, P.; Constantin, D.; Poncelet, O. Intermittent Brownian Dynamics Over a Rigid Strand: Heavily Tailed Relocation Statistics in a Simple Geometry. *Phys. Rev. E* **2008**, *78*, 030102.
(83) Chemmi, H.; Petit, D.; Korb, J.-P.; Denoyel, R.; Levitz, P. Impact of Wettability on Moisture Transport at Mesoscale in Porous Materials. *Microporous Mesoporous Mater.* **2013**, *178*, 104−107.
(84) Chemmi, H.; Petit, D.; Tariel, V.; Korb, J.-P.; Denoyel, R.; Bouchet, R.; Levitz, P. A Comprehensive Multiscale Moisture Transport Analysis: from Porous Reference Silicates to Cement-Based Materials. *Eur. Phys. J.: Spec. Top.* **2015**, *224*, 1749−1768.
(85) Chemmi, H.; Petit, D.; Levitz, P.; Denoyel, R.; Galarneau, A.; Korb, J.-P. A Noninvasive Experimental Evidence of the Linear Pore Size Dependence of Water Diffusion in Nanoconfinement. *J. Phys. Chem. Lett.* **2016**, *7*, 393−398.

DOI: 10.1021/acs.jpcc.7b09154
J. Phys. Chem. C 2017, 121, 26851−26859